Zeeman Effects in Transient Spectral Hole-Burning of the R_1 Line of $NaMgAl(Oxalate)_3 \cdot 9H_2O/Cr(III)$ in Low Magnetic Fields

Joseph L. Hughes and Hans Riesen*

School of Chemistry, University College, The University of New South Wales, Australian Defence Force Academy, Canberra, ACT 2600, Australia

Received: July 31, 2002

Transient spectral hole-burning experiments, using diode lasers, in minute external magnetic fields of <16 mT are reported for the lower-energy $^2E \leftarrow {}^4A_2$ spin-flip transition of $NaMgAl(oxalate)_3 \cdot 9H_2O/Cr(III)$. Ground- and excited-state g factors can be accurately determined by an analysis of multiple side holes observed in the selective hole-burning experiments of the $R_1(\pm 3/2)$ and $R_1(\pm 1/2)$ transitions with $B||c$ and $B \perp c$. The observed g factors, $g_z^{ex}(R_1) = 1.38 \pm 0.04$, $g_x^{ex}(R_1) = 2.00 \pm 0.08$, and $g_y^{ex}(R_1) = 1.82 \pm 0.08$, imply a large variation from trigonal behavior that is caused by a low-symmetry component of the ligand field. The zero-field hole widths in a 0.5% crystal are ~19 ± 5 MHz and 23 ± 5 MHz for holes at the low-energy edge of the $R_1(\pm 1/2)$ line and the high-energy edge of the $R_1(\pm 3/2)$ transitions, respectively. Upon application of a magnetic field of $B||c = 7$ mT, a substantial narrowing of the hole width is observed for the $R_1(\pm 1/2)$ transition, with an upper limit for the homogeneous line width of ~1 MHz. The present work illustrates the potential of diode lasers in the determination of the magnetic properties of transition-metal complexes by transient spectral hole-burning experiments in low magnetic fields.

1. Introduction

Persistent and transient spectral hole-burning experiments have been applied, with great success, to a wide range of problems in the optical spectroscopy of the solid state[1−6] since their first demonstrations[7−9] almost 30 years ago. Spectral hole-burning can overcome the inhomogeneous broadening of optical transitions in crystals and glasses by the depletion of optical centers in resonance with the laser frequency. The simplest mechanism for transient spectral hole-burning is provided by a metastable excited state with a lifetime long enough to probe the selective ground-state depletion. Excited states of transition-metal complexes involving d electrons typically have radiative lifetimes in the 10-μs−10-ms range. The frequency of conventional single-frequency dye laser systems can be scanned only relatively slowly. Thus, often two lasers are required to measure transient spectral holes,[10] or the readout is conducted by Stark[11,12] or Zeeman[13] modulation of the electronic transition of the sample with the laser kept at a constant wavelength. In contrast, laser diodes can be rapidly scanned, allowing simple hole-burning experiments to be conducted using the same laser to burn and read the hole.[14−16]

We have recently reported the temperature dependence of transient and persistent nonphotochemical hole-burning in $NaMgAl(oxalate)_3 \cdot 9H_2O/Cr(III)$.[15,16] Whereas nonphotochemical hole-burning is a common phenomenon in amorphous hosts, only a few crystalline systems have been reported to exhibit this effect.[17−20] The $[Cr(oxalate)_3]^{3-}$ complex is an archetypal complex, and rigorous investigations of its laser spectroscopy are warranted since relatively little work has been done in the class of coordination compounds. The title system lends itself to detailed studies of the $^2E \leftarrow {}^4A_2$ transitions by laser spectroscopy; compared to other chromium(III) complexes, these transitions are relatively strong, and the inhomogeneous broadening in dilute crystals is low.

The crystal structures of $NaMgAl(oxalate)_3 \cdot 9H_2O$ and $NaMgCr(oxalate)_3 \cdot 9H_2O$ are isomorphous. Early structure determinations indicated that the systems crystallize in either the $P3c1$ or $P\bar{3}c1$ trigonal space group with six formula units per unit cell.[21] Six magnetically inequivalent chromophores were indeed observed in EPR work.[22] It appears that the six sites consist of two sets of three, with an angle of 17.7° of rotation around the c axis between the two sets. The three members of each set are rotated from each other by ±120° around the crystal c axis. The x axes of the ground-state g tensor of the six chromium(III) complexes assume angles of ±8.85, 120 ± 8.85, and 240 ± 8.85° with the crystal a axis in the basal plane.

Recently, the crystal structure was reinvestigated, and it was found that the space group is indeed $P\bar{3}c1$.[23] On the basis of this space group it was concluded that the crystal may contain 10 water molecules of crystallization. However, elemental analysis performed by several groups is in the best agreement with nine water molecules of crystallization.[16,22,24] It is possible that not all positions for the water molecules are occupied in the $P\bar{3}c1$ space group, leading to disorder.

The early EPR work established the presence of a low-symmetry field by the observation of a nonzero E parameter (0.0306 cm^{-1}) in the spin Hamiltonian.[22] The $^4A_2$ ground-state splitting is relatively large, 1.6 cm^{-1}, and the ^2E splitting is 20 cm^{-1}.[21] Magnetic susceptibility measurements showed that the ±3/2 Kramers doublet of the $^4A_2$ ground state is lower in energy.[25] The absorption spectra in the region of the spin-allowed $^4T_2 \leftarrow {}^4A_2$ and $^4T_1 \leftarrow {}^4A_2$ transitions are strongly polarized. This indicates some trigonal behavior of the molecular anion despite its C_2 point symmetry in the $P\bar{3}c1$ space group. Trigonal behavior is also indicated in the relatively large zero-field splitting (zfs) of the $^4A_2$ ground state.[26]

* Corresponding author. E-mail: h.riesen@adfa.edu.au. Fax: ++61-(0)-2-6268-80-17.

10.1021/jp026646q CCC: $25.00
Published on Web 12/10/2002

In the present work, we explore the effects of minute external magnetic fields ($B||c$ and $B\perp c$) on the *transient* hole-burning spectra of the title system using free-running and pseudo-external cavity diode lasers. It is shown that the g tensor of the lowest excited state deviates strongly from trigonal behavior. We have previously reported some preliminary results regarding the observation of multiple transient holes in the R_1 line of NaMgAl(oxalate)$_3$·9H$_2$O/Cr(III) 1% in $B||c = 15$ mT.[27]

2. Experimental Section

NaMgAl(oxalate)$_3$·9H$_2$O and NaMgCr(oxalate)$_3$·9H$_2$O were prepared as described in the literature.[24,28] Mixed crystals containing 0.5−1% chromium(III) were grown from aqueous solutions by slow evaporation at room temperature. The crystals grow as hexagonal prisms along the crystal c axis. The crystals were used as taken from the mother liquor and had a typical thickness of ∼2 mm.

The samples were mounted on a sapphire window on the coldfinger of a closed-cycle refrigerator (Janis/Sumitomo SHI-4.5). Good contact with the coldfinger was achieved by embedding the crystal in heat-conducting grease (Cry-con).

Luminescence spectra were excited by an Ar^+ (488-nm line; Spectra Physics Stabilite 2017) or a He−Ne (632.8 nm) laser. The light was collimated and then modulated (Thorlabs MC1000 optical chopper) and finally dispersed by a single monochromator (Spex 1704) equipped with 1200 grooves/mm holographic gratings. In the conventional transmission experiments, the sample was exposed to the white light of a 150-W halogen lamp filtered through a 694-nm interference filter with a 10-nm bandwidth. The transmitted light was analyzed in the same way as in the luminescence experiments.

The light was detected by a cooled photomultiplier (RCA 31034C), and the photocurrent was converted by a current−voltage preamplifier (Products-For-Research PSA). The signal was then processed by a lock-in amplifier (EG&G 5210).

For the hole-burning spectra, the current and temperature of a 690-nm laser diode (Hitachi HL6738MG laser diode in a Thorlabs TCLDM9 thermolelectric mount) were stabilized by using appropriate controllers (Thorlabs LDC500 and Thorlabs TEC2000). The frequency of single-mode laser diodes can be tuned by varying the injection current. Mode-hop free scans of ∼40 GHz are possible for the diodes used in the present experiments, and the frequency/current tuning ratio is ca. −2.5 GHz/mA. The current controller (Thorlabs LDC500) allows for the external modulation of the injection current. In the transient hole-burning experiments, the current was kept constant for a time period in the 100-μs−1-ms range and then rapidly modulated by a triangular ramp provided by a wave function generator (Stanford SRS DS345). A voltage amplitude of ±10 mV corresponds to a current modulation of ±0.5 mA, translating to a frequency scan of ca. ∓1.25 GHz. The scans were calibrated by Coherent model 240 spectrum analyzers with free spectral ranges (FSRs) of 1.5 GHz and 300 MHz. Hole-burning spectra were measured in transmission, and the laser light was detected either by the photomultiplier/monochromator system described above or by a silicon photo detector (Thorlabs PDA55-EC). The signal was averaged on a digital oscilloscope (Tektronix TDS210) in the hole-burning experiments.

The line widths of the laser diodes were measured by using a spectrum analyzer (Coherent model 240) with a FSR of 300 MHz and a finesse of 320. The line width of free-running single-frequency laser diodes is inversely proportional to the optical power, as is shown for an HL6738 laser diode in Figure 1a. The laser diodes used in the present experiments had typical line widths of ∼20−40 MHz under the operating conditions.

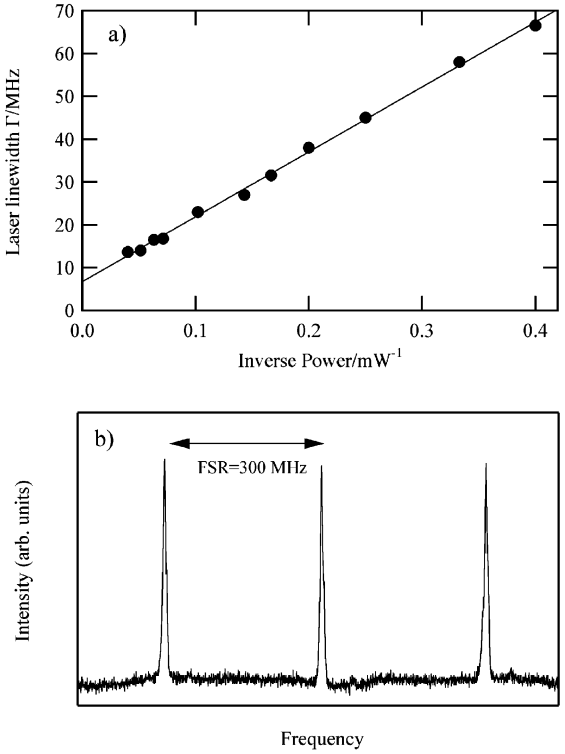

Figure 1. (a) Power dependence of the line width of a Hitachi HL6738MG laser diode at 55 °C. (b) Line width of a pseudo-external cavity laser based on the HL6738MG and a 1200-grooves/mm 750-nm blaze grating as measured by a scanning confocal Fabry−Perot interferometer with a FSR of 300 MHz and a finesse of 320. The wavelength of the laser was ∼692 nm.

The line width of diode lasers can be drastically reduced by optical feedback.[29,30] For the present work, we have built pseudo-external cavity lasers by using the optical feedback of a 1200 grooves/mm, 750-nm blazed grating in Littrow geometry. The grating was mounted on a 24.45° wedge in a piezoelectric kinematic mirror mount (Thorlabs KC1-PZ/M), allowing the first-order diffraction of the grating to be reflected back into the diode laser. The mirror mount was fixed to the thermoelectric cooler mount (TCLDM9) using (Thorlabs) cage assembly rods. The length of the external cavity was ∼25 mm. Figure 1b illustrates a line-width measurement of this laser using the spectrum analyzer with a 300-MHz FSR. The line width of 4 ± 1 MHz is most likely limited by the mechanical and thermal fluctuations of the simple cage assembly, which is not temperature-stabilized. The frequency/current tuning ratio of a pseudo-external cavity laser is dramatically reduced in comparison with that of the free-running laser: the lasers used in the present experiment showed tuning ratios of ∼300 MHz/mA.

External magnetic fields were applied by a pair of Helmholtz coils built in the laboratory. Water-cooled coil formers of 250-mm diameter were used. Each coil contained 250 turns of 1.08-mm copper wire. Two power supplies (Hewlett-Packard 6269B) connected in series provided currents of up to ∼9 A at voltages of ∼80 V. The dependence of the magnetic field on the current of the coils was 18.3 G/A as measured by a calibrated gaussmeter.

3. Results and Discussion

3.1. Polarized Luminescence and Absorption Spectra of the R Lines. In Figure 2, the polarized 2.5-K luminescence and absorption spectra of the R_1 line of NaMgAl(oxalate)$_3$·9H$_2$O/Cr(III) 0.5% are shown. When analyzing the absorption spectra, one has to take into account the Boltzmann population

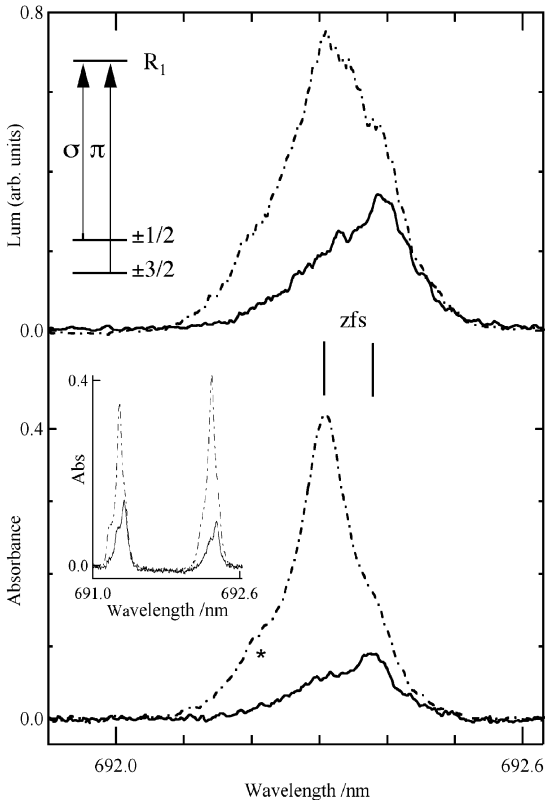

Figure 2. Polarized luminescence and absorption spectra of the R_1 line of NaMgAl(oxalate)$_3$·9H$_2$O/Cr(III) 0.5% at 2.5 K. The dashed and solid lines show π- and σ-polarized spectra, respectively. The lower inset shows the polarized absorption spectra for both R lines. The upper inset shows an energy-level diagram for the R_1 line with the predominant polarizations. The vertical bars indicate the zfs of the $^4A_2$ ground state. The asterisk denotes a transition of a minority site.

factor at 2.5 K for the $\pm 1/2$ level since the zero-field splitting is comparable to the temperature (zfs = 1.6 cm^{-1}). In contrast, the luminescence spectra display the neat intensity ratios. It follows that the R_1 transition from the $\pm 3/2$ spin level of the $^4A_2$ ground state is predominantly π-polarized. The transition from the $\pm 1/2$ level is polarized to a lesser extent but shows a strong σ component. Importantly, the ground-state splitting of 1.6 cm^{-1} is clearly visible in the absorption spectra. The observed ^2E splitting is 20 cm^{-1}, in agreement with previous reports.[15,16,21]

The integrated oscillator strength of the R lines is larger in π polarization than in σ polarization. This can be expected since the $^4T_2 \leftarrow {}^4A_2$ transition is strongly π-polarized and the $^2E \leftarrow {}^4A_2$ transitions gain intensity by the spin−orbit coupling of the ^2E and $^4T_2$ states. For example, by using eq 1, relatively high oscillator strengths of $\sim 1 \times 10^{-6}$ and 8×10^{-7} are obtained for the π component of the R_1 and R_2 lines, respectively.

$$f = 4.3 \times 10^{-9} \int \epsilon(\bar{\nu})\, \mathrm{d}\bar{\nu} \qquad (1)$$

These values are approximately an order of magnitude higher than those commonly observed for the $^2E \leftarrow {}^4A_2$ transitions of chromium(III) coordination compounds.[31] The relative transition dipole strengths for the R lines are given in Table 1 for trigonal symmetry.[32] Although some aspects of Table 1 are observed in the polarized absorption spectrum, the overall agreement is poor. For example, a ratio of 3:1 is expected in π polarization for the two lines. This is not observed. In particular, the R_2 transition dipole strengths deviate from any predicted pattern.

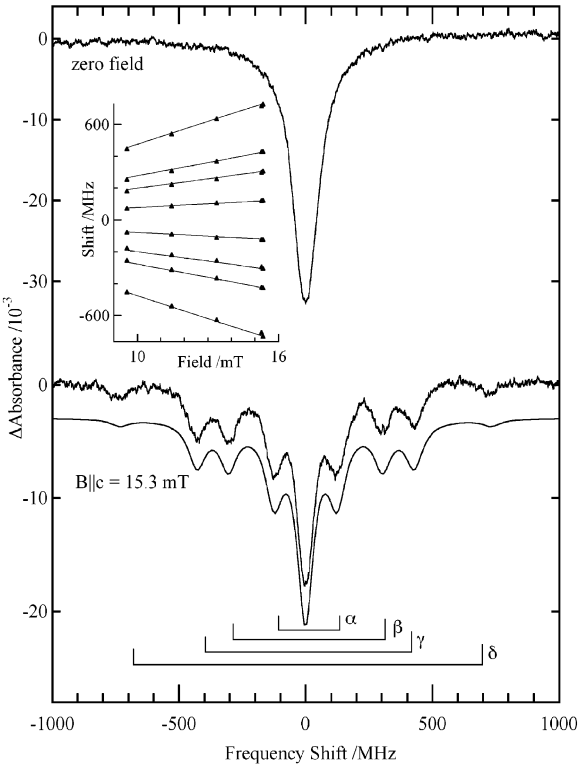

Figure 3. Transient spectral hole-burning at the red edge (692.37 nm) of the R_1 line in NaMgAl(oxalate)$_3$·9H$_2$O/Cr(III) 1% at 2.5 K. The top trace shows the hole-burning spectrum in zero field; the bottom traces compare the experimental hole-burning spectrum in $B||c = 15.3$ mT with a fit by a sum of Lorentzians (smooth line) using $A_0(\sigma)/A_1(\sigma) = 3.3$, $g_z = 1.99$; $g_z^{ex} = 1.42$, $\Gamma_{rh} = 76$ MHz, $\Gamma_{sh} = 84$ MHz. The inset summarizes the hole shifts as a function of $B||c$ in the range of 10−16 mT. The σ-polarized laser light was detected by a photomultiplier. The spectrum is the average of 2056 readouts (0.5-ms readout period, 1-kHz repetition rate of burn-read cycle).

TABLE 1: Trigonal Transition Dipole Strengths for the $\langle {}^2E, M_s', M'| \leftarrow \langle {}^4A_2, M_s|$ Transitions[32]

M_s	$M_s', M'=$	1/2, u+	−1/2, u−	−1/2, u+	1/2, u−
3/2		$\pi/2$			$\sigma+/2$
1/2		$\sigma+/3$	$\sigma+/6$	$\pi/6$	$\sigma-/3$
−1/2		$\sigma-/6$	$\sigma-/3$	$\sigma+/3$	$\pi/6$
−3/2			$\pi/2$	$\sigma-/2$	

The asterisk in Figure 2 denotes a feature that must be due to a minority site that is not part of the six magnetically inequivalent sites. Further work is needed to determine the nature of this feature.

3.2. Transient Hole-Burning Spectroscopy with *B*||*c*. Although the zero-field splitting of the $^4A_2$ ground state is not completely resolved in the absorption spectrum of the R_1 line, the polarization allows selective transient hole-burning experiments. When the laser light is σ-polarized and at the red edge of the R_1 line, the sample gets predominantly excited via the $R_1(\pm 1/2)$ transition (originating from the $\pm 1/2$ spin level in the ground state); when the laser light is at the blue edge and π-polarized, the $R_1(\pm 3/2)$ transition is selected. This selectivity simplifies the side-hole patterns observed in the Zeeman hole-burning studies, as is discussed below.

Figure 3 shows transient hole-burning spectra in zero field and for $B||c = 15.3$ mT at the red edge of the R_1 line in a NaMgAl(oxalate)$_3$·9H$_2$O/Cr(III) 1% crystal. The laser light was σ-polarized and hence selects the $R_1(\pm 1/2)$ transition(s). The spectrum in 15.3 mT shows four pairs of side holes. These side

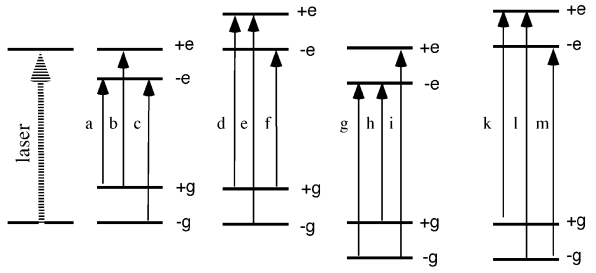

Figure 4. Schematic energy diagram for the R_1 transitions from the $^4A_2$ $M_s = \pm 1/2$ or $M_s = \pm 3/2$ levels in an external magnetic field. The ground- and excited-state magnetic spin quantum numbers are denoted as $\pm$g and $\pm$e, respectively. The laser is in resonance with four subsets of chromium(III) complexes.

TABLE 2: Notation for Energy Splitting of Side-Hole Pairs

α	$2 \times$ |(ground-state splitting $-$ excited-state splitting)|
β	$2 \times$ excited-state splitting
γ	$2 \times$ ground-state splitting
δ	$2 \times$ (ground-state splitting $+$ excited-state splitting)

holes arise from the Zeeman splittings of the ground and excited states and can be rationalized by the four-level diagram shown in Figure 4.

In particular, side holes are expected on both sides of the resonant hole with frequency shifts corresponding to the ground-state splitting (transitions b, f, i, and m), the excited-state splitting (c, e, h, and k), and the sum (transitions a and l) and difference (transitions d and g) of the two splittings. The energy splitting of each pair is denoted (see Figure 3) according to Table 2.

The effective spin Hamiltonian for the $^4A_2$ ground state of chromium(III) is given by eq 2.[33]

$$H = D\left[S_z^2 - \frac{1}{3}S(S+1)\right] + E(S_x^2 - S_y^2) + \mu_B \mathbf{B}\cdot\mathbf{g}\cdot\mathbf{S} + \mathbf{I}\cdot\mathbf{A}\cdot\mathbf{S} \quad (2)$$

In the following equations, we neglect the hyperfine term in eq 2 since 90.5% of the stable chromium(III) isotopes have no nuclear spin. The eigenvalues of the Hamiltonian in eq 2 for magnetic fields parallel to the molecular z axis are given by

$$E(\pm 1/2) = \mp 1/2\mu_B B_z g_z - ((D \mp \mu_B B_z g_z)^2 + 3E^2)^{1/2} \quad (3)$$

$$E(\pm 3/2) = \pm 1/2\mu_B B_z g_z + ((D \pm \mu_B B_z g_z)^2 + 3E^2)^{1/2} \quad (4)$$

where μ_B is the Bohr magneton and B_z is the strength of the magnetic field along the z axis. For the present system, the parameters $D = -0.7786$ cm^{-1} and $E = 0.0306$ cm^{-1} were determined by EPR spectroscopy and magnetic susceptibility measurements.[22,25] The rhombic parameter is relatively small, and its effect on the eigenvalues is $<0.5\%$. Thus, the eigenvalues in a small external magnetic field are well approximated by eqs 5 and 6, where |zfs| is $2(D^2 + 3E^2)^{1/2} \approx 2|D|$.

$$E(\pm 1/2) \approx \pm 1/2\mu_B B_z g_z + |\text{zfs}|/2 \quad (5)$$

$$E(\pm 3/2) \approx \pm 3/2\mu_B B_z g_z - |\text{zfs}|/2 \quad (6)$$

The excited-state splitting of the lower ^2E level is given by $\mu_B B_z g_z^{ex}$. Thus, side holes are expected at $\pm\mu_B B_z g_z$ for i, m, b, and f (γ pair); at $\pm\mu_B B_z g_z^{ex}$ for e, k, c, and h (β pair); at $\pm\mu_B B_z (g_z + g_z^{ex})$ for l, a (δ pair); and at $\pm\mu_B B_z (g_z - g_z^{ex})$ for g and d (α pair). The change in optical density of each member of a side-hole pair in comparison with the resonant hole is parametrized in Table 3. This parametrization takes into account

TABLE 3: Patterns of ΔA for Multiple Holes in an External Magnetic Field for the $R_1(\pm 3/2)$ and $R_1(\pm 1/2)$ Lines in Terms of Transition Dipole Strengths A_0 ($\Delta M_s = 0$), A_1 ($\Delta M_s = \pm 1$, $R_1(\pm 1/2)$), A'_1 ($\Delta M_s = \pm 1$, $R_1(\pm 3/2)$), and A_2 ($\Delta M_s = \pm 2$)

hole shift	ΔA $R_1(\pm 1/2)$	ΔA $R_1(\pm 3/2)$
0 (resonant)	$2A_0^2 + 2A_1^2$	$2A'^2_1 + 2A_2^2$
$\pm\alpha/2$	A_0^2	A'^2_1
$\pm\beta/2$	$2A_0A_1$	$2A'_1A_2$
$\pm\gamma/2$	$2A_0A_1$	$2A'_1A_2$
$\pm\delta/2$	A_1^2	A_2^2

that hole-burning is a sequential two-photon experiment. The first photon is used to burn the hole, and the second photon is used in the readout process. The absorbance changes are expressed in terms of transition dipole strength parameters for $\Delta M_s = 0$, ± 1, and ± 2.

An excellent fit of the hole-burning spectrum in Figure 3 is provided by a sum of nine Lorentzians using the parameters $g_z = 1.99$, $g_z^{ex} = 1.42$, and $A_1(\sigma)/A_0(\sigma) = 0.30$, where $A_1(\sigma)$ and $A_0(\sigma)$ are the $\Delta M_s = 1$ and 0 transition dipole strengths in σ polarization, respectively, and a width for the resonant hole, $\Gamma_{rh} = 76$ MHz, and for the side holes, $\Gamma_{sh} = 84$ MHz. The side holes are about 8 MHz broader than the resonant feature. We assign this difference to g strain, that is, some inhomogeneous distribution of the g factors. Both the excited-state and the ground-state g strain are likely to contribute to the extra width.

The inset of Figure 3 summarizes the observed splittings $\alpha - \gamma$ of all side-hole pairs with linear fits, providing an average g_z^{ex} factor of 1.38 ± 0.04.

By using Table 1, a ratio of the transition dipole strengths $A_1(\sigma)/A_0(\sigma)$ of 0.5 is predicted if the $2\bar{A}$ Kramers doublet is the lower ^2E level, whereas for the $\bar{E}$ level no σ intensity is expected for the $\Delta M_s = \pm 1$ transitions. Thus, the observed ratio indicates that the lower ^2E level has some $2\bar{A}$ parentage. The deviation from the predicted patterns indicates again that the low-symmetry field must strongly influence the $^2E \leftarrow {}^4A_2$ transitions.

The observed hole widths in Figure 3 are dominated by the laser line width. Figure 5 shows transient hole-burning spectra measured with a pseudo-external cavity laser with a line width of $\sim$4 MHz. The zero-field hole width is $\sim$27 MHz, whereas the narrowest resonant holes in 15.3 mT observed in single-shot experiments are $\sim$8 MHz. Because of the two-photon nature of the hole-burning phenomenon, the observed hole width is composed of twice the "homogeneous" line width and the laser line width, $\Gamma_{hole} = 2\Gamma_{homogeneous} + 2\Gamma_{laser}$, if the line shapes of the transitions and the laser are Lorentzian. Hence, the zero-field hole width is $\sim$19 MHz after correction for the laser line width, and the homogeneous line width in a field of 15 mT must be less than $\sim$1 MHz. The zero-field width of 19 MHz is substantially narrower than the previously reported widths of 90 MHz for a 4% crystal and 40 MHz for a 1% crystal.[15,16,27] The crystal used in the experiments illustrated in Figure 5 had a chromium(III) concentration of 0.5%. The concentration dependence indicates that indirect electron spin$-$spin interactions make a substantial contribution to the hole width for higher concentrations. It is possible that this is still the case in the 0.5% crystal (9.4×10^{18} chromium(III) centers/cm^3).[34,35]

The lower panel in Figure 5 shows that a minute magnetic field of $B||c = 2.2$ mT is sufficient to resolve all side holes fully in these higher-resolution experiments (δ pair not shown).

Transient spectral hole-burning experiments in magnetic fields $B||c$ at the blue edge of the R_1 line are illustrated in Figures 6 and 7. The energy spacings in the side-hole pattern are quite different in comparison with red-edge excitation since the R_1-

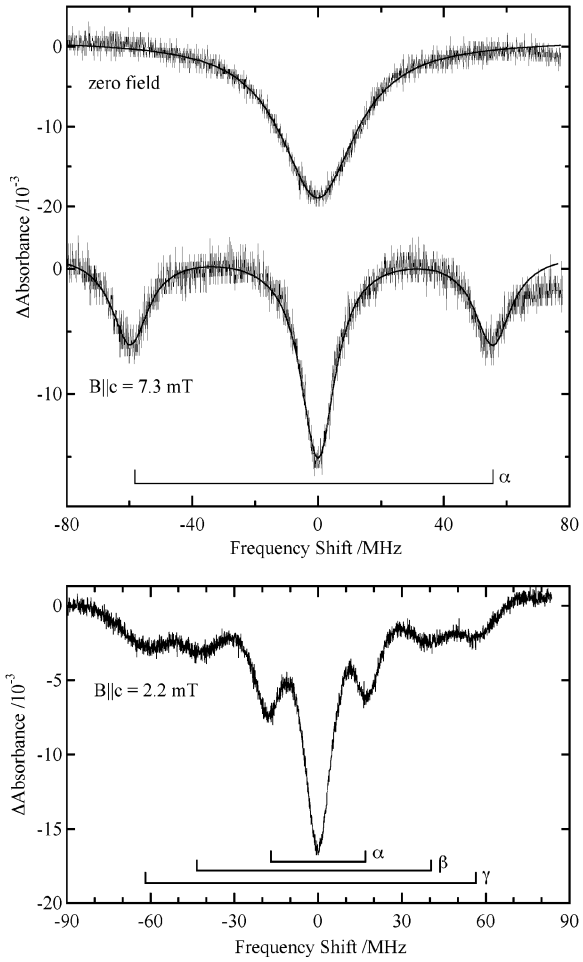

Figure 5. Transient spectral hole-burning in $NaMgAl(oxalate)_3 \cdot 9H_2O$/Cr(III) 0.5% at 2.5 K using a pseudo-external cavity diode laser at 692.33 nm (red edge of the R_1 line) in σ polarization. In the upper panel, spectra are shown for zero field and $B||c = 7.3$ mT. The frequency of the laser was tuned over 180 MHz by modulating the injection current. The transmitted laser light was detected by a Si photodetector. The smooth lines in the upper panel are Lorentzian fits with hole widths, Γ_{hole}, of 27 and 12 MHz for the zero-field and 7.3-mT data, respectively. The laser scan was calibrated using the positions of the side holes in the 7.3-mT spectrum. The lower panel shows a 180-MHz scan in $B||c = 2.2$ mT. The spectra in the upper and lower panels are the averages of 16 and 1024 readouts, respectively (0.2-ms readout period, 1-kHz repetition rate of burn-read cycle).

($\pm 3/2$) transition is selected in these experiments with π-polarized laser light. The magnetic-field splitting of the $\pm 3/2$ ground-state spin component is 3 times as large as that of the $\pm 1/2$ level, leading to a change in the sequence of the $\alpha-\gamma$ side-hole pairs to β, α, γ, and δ. As is illustrated in Figure 6, the hole-burning spectrum can again be well described by a sum of nine Lorentzians with the parameters $g_z^{ex} = 1.40$, $g_z = 1.92$, $\Gamma_{rh} = 63$ MHz, and $\Gamma_{sh} = 76$ MHz. A ratio $A_2(\pi)/A'_1(\pi)$ of 0.24 is obtained by a nonlinear least-squares fit. The difference in width between the side holes and the resonant hole again implies the presence of some inhomogeneous distribution in the g factors. The insert in Figure 6 summarizes the data of the pair splittings with the exception of δ, which in this case is hard to measure because of the low transition dipole strength involved. From this data, an average g_z^{ex} factor of 1.38 ± 0.04 results in agreement with the analysis of the hole spectra in the $R_1(\pm 1/2)$ line. We note here that trigonal selection rules are severely violated by the nonzero $\Delta M_s = \pm 2$ transition dipole strength $A_2(\pi)$.

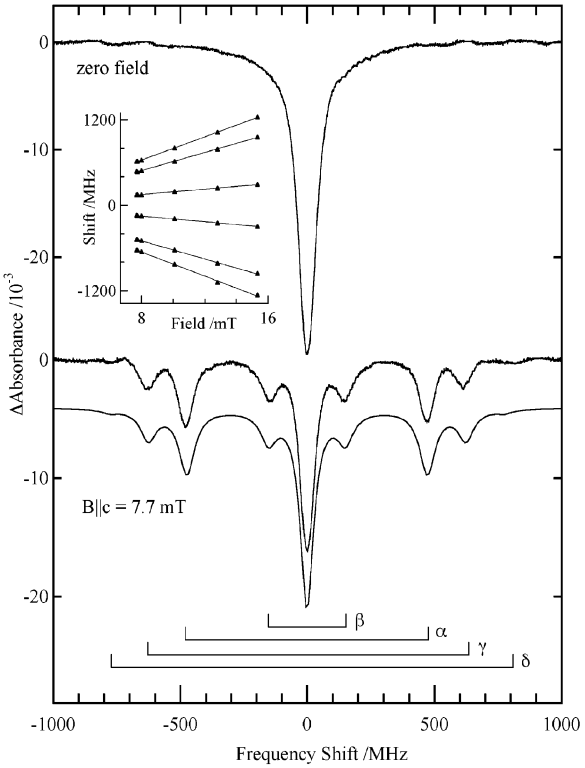

Figure 6. Transient spectral hole-burning at the blue edge (692.24 nm) of the R_1 line in $NaMgAl(oxalate)_3 \cdot 9H_2O$/Cr(III) 0.5% at 2.5 K. The top trace shows the hole-burning spectrum in zero field; the bottom traces compare the experimental hole-burning spectrum in $B||c = 7.73$ mT with a fit by a sum of Lorentzians (smooth line) using the parameters $A_2(\pi)/A'_1(\pi) = 0.24$ and $g_z = 1.92$; $g_z^{ex} = 1.40$, $\Gamma_{rh} = 63$ MHz, $\Gamma_{sh} = 76$ MHz. The inset summarizes the hole shifts as a function of the applied magnetic field, $B||c$, in the range of 7−16 mT. The laser light was π-polarized and detected by a Si photodiode. The spectra are the average of 2056 readouts (0.2-ms readout period, 3-kHz repetition rate of burn-read cycle).

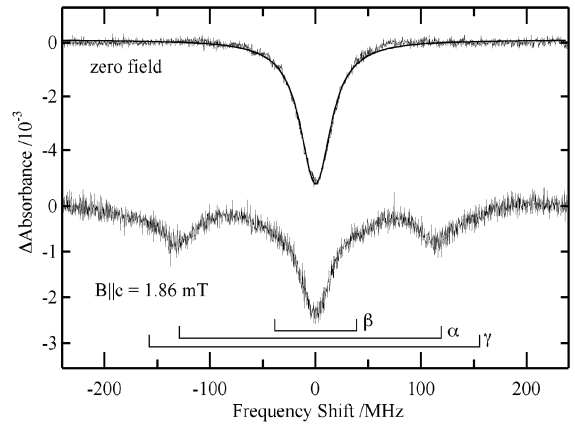

Figure 7. Transient spectral hole-burning in $NaMgAl(oxalate)_3 \cdot 9H_2O$/Cr(III) 0.5% at 2.5 K with a pseudo-external cavity laser at 692.26 nm (blue edge of the R_1 line) in π polarization. Spectra are shown for zero field and $B||c = 1.86$ mT and are the averages of 2056 readouts. The frequency of the laser was tuned over ~400 MHz by modulating the injection current. The transmitted laser light was detected by a Si photodetector. The smooth line (zero-field spectrum) is a fit to a Lorentzian with a hole width of $\Gamma_{hole} = 35$ MHz.

The average ground-state g_z factor observed in these experiments is 1.94 ± 0.04. The hole-burning experiments in the R_1-($\pm 1/2$) line, as summarized in Figure 3, indicate a ground-state value of 1.96 ± 0.04. Although these values are in reasonable agreement with the reported room-temperature g_z factor of 1.98

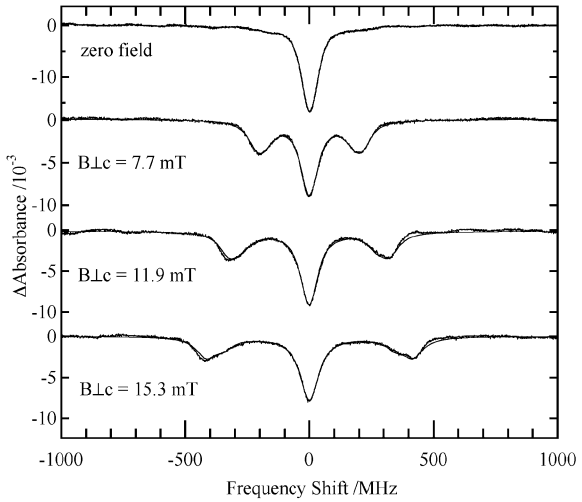

Figure 8. Transient spectral hole-burning at the blue edge (692.24 nm) of the R_1 line in $NaMgAl(oxalate)_3 \cdot 9H_2O/Cr(III)$ 0.5% at 2.5 K in magnetic fields $B \perp c(\varphi = 60°)$ of 7.7, 11.9, and 15.3 mT. The top trace shows the hole-burning spectrum in zero field. The experimental spectra are compared with fits (smooth lines) as discussed in the text. The laser light was π-polarized and detected by a Si photodiode. The spectra are averages of 2056 readouts (0.2-ms readout period, 3-kHz repetition rate of burn-read cycle).

obtained by EPR work,[22] it is possible that the g tensor is slightly temperature-dependent.

Figure 7 displays the results of experiments with a pseudo-external cavity diode laser at higher resolution. The narrowest hole widths observed in zero field and 15.3 mT were 23 ± 5 MHz and 14 ± 5 MHz, respectively (corrected for the laser line width). In comparison with the results for the $R_1(\pm 1/2)$ transition, these holes are significantly broader. This may be due to the larger magnetic dipole interactions associated with the ±3/2 spin components.

3.3. Transient Hole-Burning Spectroscopy with $B \perp c$. Figure 8 illustrates transient spectral hole-burning experiment at the blue edge of the R_1 line in external magnetic fields perpendicular to the c axis, $B \perp c$. The crystal was mounted on a $(1\bar{1}00)$ face, resulting in an angle between the magnetic field and the crystal a axis, φ, of 60°. In contrast to the experiments with $B||c$, we have to take into account that there are, in principle, six magnetically inequivalent sites. By applying the spin Hamiltonian of eq 2 with the experimental geometry (θ = 90°, φ = 60°), it follows that there are three pairs of chromophores with the same ground-state splitting. The ground-state splitting is not a linear function of the magnetic field for these experiments since the Zeeman interaction terms are off-diagonal in the matrix given by eq 2. The splitting for the ±3/2 spin level is very small, with $B \perp c \approx 15$ mT. Applying g_x = 1.9822, g_y = 1.9812, $D = -0.7786$ cm^{-1}, and $E = 0.0306$ cm^{-1}, which are values determined by EPR work,[22] the splitting of the ±3/2 level is calculated to vary from 49 to 51 MHz (in 15.3 mT) for the three pairs of chromophores in the experimental geometry. Consequently, the side holes that are well separated from the resonant hole in the experimental results shown in Figure 8 must be due to the excited-state splitting, and thus $g^{ex} \perp c \neq 0$. For a trigonal species, there would be no excited-state splitting in first order since the Zeeman operator has only matrix elements between the $2\bar{A}$ and $\bar{E}$ levels; these levels are separated by 20 cm^{-1} in the title system. Thus, it follows that low-symmetry fields govern the g factors of the ^2E levels. The shifts of the side holes as observed in Figure 8 indicate that $g^{ex} \perp c \approx 1.9 \pm 0.2$. The line shape of the side holes also indicates that there is ~10% anisotropy, implying $g_x^{ex} \neq g_y^{ex}$.

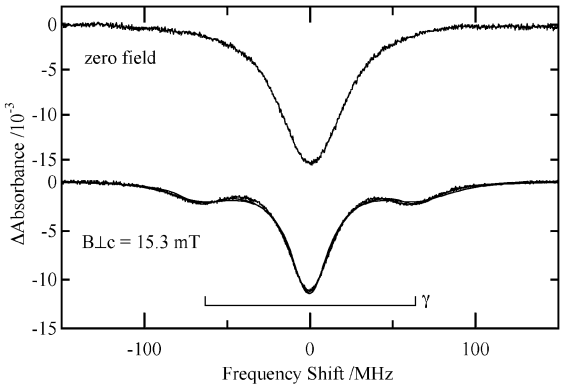

Figure 9. Transient spectral hole-burning at the blue edge (692.24 nm) of the R_1 line in $NaMgAl(oxalate)_3 \cdot 9H_2O/Cr(III)$ 0.5% at 2.5 K using a pseudo-external cavity laser. The zero-field and $B \perp c(\varphi = 60°)$ = 15.3 mT spectra are compared. The fit is the sum of three Lorentzians with a 30-MHz width and a ground-state splitting of 66 MHz. The laser light was π-polarized and detected by a Si photodiode. The spectra are averages of 2056 readouts (0.2-ms readout period, 3-kHz repetition rate of burn-read cycle).

In principle, the spectrum can be analyzed in terms of the schematic diagram shown in Figure 4. Since the ground-state splitting is only about 50 MHz, each side hole observed in Figure 8 is composed of nine transitions (three side holes for each magnetically inequivalent chromophore: α, β, and δ). Because the line width of the laser used for these experiments was ~50 MHz, the ground-state splitting was neglected in the fit of the data. The hole-burning spectrum is then the sum of the spectra of the three pairs of chromophores whose effective excited-state g factor is given by eq 7:

$$g^{\text{eff}}(\varphi') = ((g_x^{\text{ex}})^2 \cos^2(\varphi') + (g_y^{\text{ex}})^2 \sin^2(\varphi'))^{1/2} \qquad (7)$$

where φ' = (−68.85°, 68.85°), (−51.15°, 51.15°), or (171.15°, 188.85°) is the angle between the magnetic field and the x axis of the ground-state g tensor in the basal plane of the crystal.

Each pair of chromophores will lead to side holes at $\pm g^{\text{eff}}(\varphi')\mu_B B \perp c(\varphi')$. Since the ground-state splitting is neglected, the ratio of ΔA of the resonant hole and each side hole is 2:1 for each chromophore. The hole shapes in Figure 8 are again approximated by Lorentzians. The data do not allow unambiguous discrimination between g_x^{ex} and g_y^{ex}. From the fits displayed in Figure 8, we obtain $g_x^{\text{ex}} = 2.02 \pm 0.07$ and $g_y^{\text{ex}} = 1.80 \pm 0.07$, or vice versa. The indicated error is a conservative estimate, taking into account experimental uncertainties in the laser frequency scan and the magnetic field strength. The widths for the central hole and the side holes are 85 and 95 MHz, respectively. Again, the extra width of 10 MHz of the side holes is assigned to g strain in the ground and the excited states.

Higher resolution hole-burning spectra, using a pseudo-external cavity laser, are shown in Figure 9. The ground-state splitting of the ±3/2 level is clearly observed in a field of 15.3 mT. Since this splitting varies only by ~1 MHz for the three pairs of chromophores, the spectrum is well described by a resonant hole and two side holes. The observed splitting is ~66 MHz, whereas the parameters determined by EPR spectroscopy predict a splitting of ~50 MHz for the ±3/2 spin levels in 15.3 mT (see above). This variation may be due to a minor misalignment of the crystal with respect to the external magnetic field. For example, using the EPR parameters, a splitting of 66 MHz is calculated when the magnetic field is out of the basal plane by 2°. However, we cannot fully exclude the possibility that the g tensor and the zfs parameters are slightly temperature-

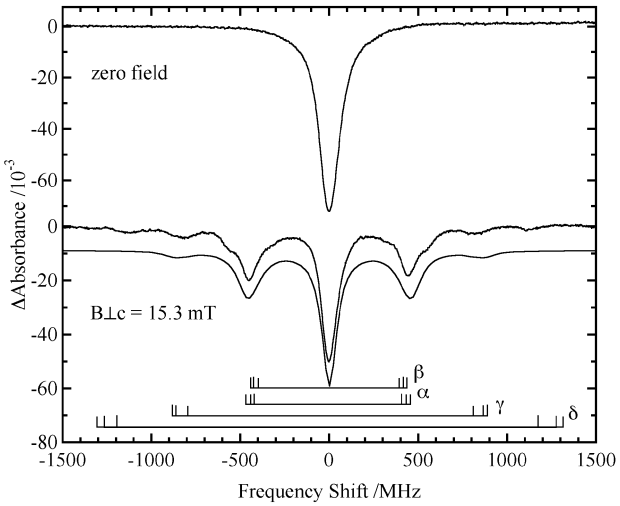

Figure 10. Transient spectral hole-burning at the red edge (692.38 nm) of the R_1 line in $NaMgAl(oxalate)_3 \cdot 9H_2O/Cr(III)$ 0.5% at 2.5 K. The zero-field spectrum is compared with the spectrum obtained in a magnetic field of $B \perp c(\varphi = 60°) = 15.3$ mT. The fit (smooth line with offset) is discussed in the text. The laser light was σ-polarized and detected by a photomultiplier. The spectra are averages of 2056 readouts (0.2-ms readout period, 3-kHz repetition rate of burn-read cycle).

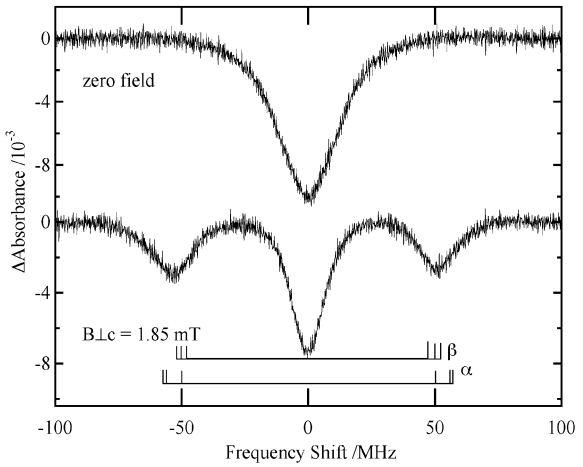

Figure 11. Transient spectral hole-burning at the red edge (692.38 nm) of the R_1 line in $NaMgAl(oxalate)_3 \cdot 9H_2O/Cr(III)$ 0.5% at 2.5 K using a pseudo-external cavity laser. The zero-field spectrum is compared with the spectrum obtained in a magnetic field $B \perp c(\varphi = 60°) = 1.85$ mT. The laser light was σ-polarized and detected by a Si photodiode. The spectra are averages of 2056 readouts (0.2-ms readout period, 3-kHz repetition rate of burn-read cycle).

dependent and thus different from those observed in the room-temperature EPR work. For example, an increase of the rhombic parameter E by 35% leads to a splitting of the $\pm 3/2$ level of $\sim$65 MHz in 15.3 mT using the same g factors. At room temperature, E is relatively small (0.0306 cm^{-1}), and it is possible that the contraction of the lattice with decreasing temperature increases the lower-symmetry field. Of course, both factors may contribute to the variation of the splitting.

The transient hole-burning spectra with $B \perp c$ are somewhat different for red-edge excitation, as is illustrated in Figure 10 where the magnetic field was applied in the direction of the light propagation; that is, the angle φ between $B \perp c$ and the crystal a axis was 150°. In the simulation of these experiments, we have to take into account the relatively large ground-state splitting of the $\pm 1/2$ level. The angles φ' between the x axis and the magnetic field $B \perp c$ of the three pairs of equivalent chromophores are (−158.85°, −21.15°), (−141.15°, −38.85°), and (81.18°, 98.85°). In $B \perp c(\varphi')$ = 15.3 mT, ground-state splittings of 888, 862, and 802 MHz, respectively, result for these pairs. The analysis of the hole-burning data follows the procedure as outlined above for the $B||c$ experiments, but the spectrum is the sum of the contributions of the three pairs of chromophores with individual ground-state splittings. The factors $g_x^{ex} = 1.98 \pm 0.08$ and $g_y^{ex} = 1.84 \pm 0.08$ are obtained from the nonlinear least-squares fit displayed in Figure 10. This is in good agreement with the results for the $R_1(\pm 3/2)$ experiments discussed above. Furthermore, this experiment appears to distinguish between g_x^{ex} and g_y^{ex}. Again, the indicated error is a conservative estimate taking into account the experimental accuracy.

A ratio of the intensities $A_0(\sigma)/A_1(\sigma) = 12$ results from the fit of the data in Figure 10. This is in accord with a simple model calculation using the eigenvectors in the magnetic field $B \perp c$ of the levels involved.

Figure 11 shows a higher-resolution hole-burning spectrum measured with the pseudo-external cavity laser. Selecting the $R_1(\pm 1/2)$ transition at the red edge (692.38 nm), a field of $B \perp c$ = 1.85 mT is sufficient to separate the side holes fully from the resonant hole. The observed widths are 27 MHz in zero field and 14 MHz for the resonant hole in 1.85 mT. Single-shot experiments again indicate, as in the $B||c$ = 7 mT experiments, that the hole width is basically limited by the laser line width.

4. Conclusions

Transient spectral hole-burning experiments in *minute* external magnetic fields allow for the determination of g factors of the lower-energy level of the ^2E multiplet in the title compound. For example, the g_z factors of the ground and first excited states can be fully determined from the observation of multiple holes in a field as low as $B||c = 2.2$ mT. The g factors with $B \perp c$ are close to spin-only and hence indicate that the electronic structure of the intrinsically trigonal $[Cr(oxalate)_3]^{3-}$ complex is subject to a significant low-symmetry perturbation. The pattern of multiple holes can be well simulated by a four-level model. We note here that Zeeman experiments of the R_2 line would also be feasible. However, for this transition, a magnetic field approximately 10 times stronger would be required since the transient hole width is substantially larger.[16]

Upon the application of low magnetic fields $B||c$, a significant narrowing of the $R_1(\pm 1/2)$ transitions results, and the observed hole width is basically determined by the laser line width; it follows that the homogeneous line width of these transitions must be less than $\sim$1 MHz in 15 mT. In comparison, zero-field widths of 19 and 23 MHz are observed for the $R_1(\pm 1/2)$ and $R_2(\pm 3/2)$ transitions, respectively. The magnetic field effect shows that the hole widths are governed by magnetic dipole interactions. The concentration of the chromium(III) centers in the present experiments was still relatively high (9.4×10^{18}/cm^3), and thus *indirect* electron spin−spin interactions may well be a major factor for these widths.[34,35] However, it is also very likely that superhyperfine interactions with the ^{27}Al and ^1H nuclear spins will contribute to the residual hole widths. We are currently addressing this question by investigations of deuteration effects and by lowering the chromium(III) concentrations further. Since the zero-field hole widths are substantially narrower than in ruby, it is possible that extremely narrow hole widths may be observed in moderate fields of several hundred mT. In comparison with ruby, the advantage of the title system lies in the fact that the chromium(III) does not share any ligands with the aluminum(III) ion. Hence, superhyperfine interactions with ^{27}Al should be reduced.

The present work establishes the potential of inexpensive diode lasers in the spectroscopy of coordination compounds in the solid state. Because of their inherent intensity stability, it is possible to read out very shallow holes with an extremely good signal-to-noise ratio. For example, holes with a change in the optical density of $\Delta A = 1 \times 10^{-3}$ are readily measurable. The present work also points to possible applications of the title system and related compounds in stabilization schemes for semiconductor lasers by spectral hole-burning [36] and possible Zeeman scanning of the laser frequency.[37]

Acknowledgment. This work was supported by the Australian Research Council (large grant scheme grant no. A00104371). We thank K. Piper, K. Richens, and S. Cheney for their technical support.

References and Notes

(1) *Persistent Spectral Hole-Burning: Science and Applications;* Moerner, W. E., Ed.; Topics in Current Physics; Springer-Verlag: Heidelberg, Germany, 1988; Vol. 44.
(2) *Laser Spectroscopy of Solids;* Yen, W., Selzer, P. M., Eds.; Topics in Applied Physics; Springer-Verlag: Berlin, 1981; Vol. 49.
(3) Meltzer, R. S.; Yen, W. M.; Zheng, H. R.; Feofilov, S. P.; Dejneka, M. J.; Tissue, B.; Yuan, H. B. *J. Lumin.* **2001**, *94*, 221.
(4) Skinner, J. L.; Moerner, W. E. *J. Phys. Chem.* **1996**, *100*, 13251.
(5) MacFarlane, R. M.; Shelby, R. M. In *Spectroscopy of Solids Containing Rare Earth Ions*; Kaplyanskii, A. A., Macfarlane, R. M., Eds.; Elsevier Science Publishers: Amsterdam, 1987; pp 51−184.
(6) Rebane, K. K. *J. Lumin.* **2000**, *86*, 167.
(7) Gorokhovskii, A. A.; Kaarli, R. K.; Rebane, L. A. *JETP Lett. (Engl. Transl.)* **1974**, *20*, 216.
(8) Kharlamov, B. M.; Personov, R. I.; Bykovskaya, L. A. *Opt. Commun.* **1974**, *12*, 191.
(9) Szabo, A. *Phys. Rev. B* **1975**, *11*, 4512
(10) Riesen, H.; Wallace, L.; Krausz, E. *Inorg. Chem.* **2000**, *39*, 5044.
(11) Muramoto, T.; Nakanishi, S.; Hashi, T. *Opt. Commun.* **1977**, *21*, 139.
(12) Riesen, H.; Krausz, E. *Chem. Phys. Lett.* **1993**, *212*, 347.
(13) Wang, Y. P.; Landau, D. P.; Meltzer, R. S.; Macfarlane, R. M. *J. Opt. Soc. Am. B* **1992**, *9*, 946.
(14) Wannemacher, R.; Smorenburg, H. E.; Schmidt, T.; Völker, S. *J. Lumin.* **1992**, *53*, 266.
(15) Lewis, M. L.; Riesen, H. *PhysChemComm* **2001**, *26*, 1.
(16) Lewis, M. L.; Riesen, H. *J. Phys. Chem. A* **2002**, *106*, 8039.
(17) Holliday, K.; Manson, N. B. *J. Phys.: Condens. Matter* **1989**, *1*, 1339.
(18) Reeves, R. J.; Macfarlane, R. M. *J. Opt. Soc. Am. B* **1992**, *9*, 763.
(19) Macfarlane, R. M.; Reeves, R. J.; Jones, G. D. *Opt. Lett.* **1987**, *12*, 660.
(20) Riesen, H.; Bursian, V. E.; Manson, N. B. *J. Lumin.* **1999**, *85*, 107.
(21) Mortensen, O. S. *J. Chem. Phys.* **1967**, *47*, 4215.
(22) Bernheim, R. A.; Reichenbecher, E. F. *J. Chem. Phys.* **1969**, *51*, 996.
(23) Suh, J.-S.; Shin, J.-Y.; Yoon, C.; Lee, K.-W.; Suh, I.-H.; Lee, J.-H.; Ryu, B.-Y.; Lim, S.-S. *Bull. Korean Chem. Soc.* **1994**, *15*, 255.
(24) Piper, T. S.; Carlin, R. L. *J. Chem. Phys.* **1961**, *35*, 1809.
(25) Lahiry, S.; Kakkar, R. *Chem. Phys. Lett.* **1982**, *88*, 499.
(26) Dubicki, L. *Comments Inorg. Chem.* **1991**, *12*, 35.
(27) Hughes, J. L.; Riesen, H. *Chem. Commun.* **2002**, 1616.
(28) Frossard, L. *Schweiz. Mineral. Petrogr. Mitt.* **1956**, *35*, 1.
(29) Wieman, C. E.; Hollberg, L. *Rev. Sci. Instrum.* **1991**, *62*, 1.
(30) MacAdam, K. B.; Steinbach, A.; Wieman, C. *Am. J. Phys.* **1992**, *60*, 1098.
(31) Sugano, S.; Tanabe, Y.; Kamimura, H. *Multiplets of Transition-Metal Ions in Crystals;* Pure and Applied Physics; Academic Press: New York, 1970; Vol. 33.
(32) Sugano, S.; Tanabe, Y. *J. Phys. Soc. Jpn.* **1958**, *13*, 880.
(33) Abragam, A.; Pryce, M. H. L. *Proc. R. Soc. London, Ser. A* **1951**, *205*, 135.
(34) Szabo, A.; Kaarli, R. *Phys. Rev. B* **1991**, *44*, 12307.
(35) Szabo, A.; Muramoto, T.; Kaarli, R. *Phys. Rev. B* **1990**, *42*, 7769.
(36) Sellin, P. B.; Strickland, N. M.; Carlsten, J. L.; Cone, R. L. *Opt. Lett.* **1999**, *24*, 1038.
(37) Clifford, A. A.; Lancaster, G. P. T.; Conroy, R. S.; Dholakia, K. *J. Mod. Opt.* **2000**, *47*, 1933.